Available online at www.sciencedirect.com
SCIENCE DIRECT®
Journal of Molecular Catalysis A: Chemical 230 (2005) 69–77
JOURNAL OF MOLECULAR CATALYSIS A: CHEMICAL
www.elsevier.com/locate/molcata

Effect of promoters on the structures and properties of the RuB/γ-Al_2O_3 catalyst

Ge Luo, Shirun Yan*, Minghua Qiao, Kangnian Fan*

Department of Chemistry and Shanghai Key Laboratory of Molecular Catalysis and Innovative Materials, Fudan University, 220 Handan Road, Shanghai 200433, PR China

Received 25 August 2004; received in revised form 17 December 2004; accepted 17 December 2004
Available online 19 January 2005

Abstract

Effect of promoters (Co, Fe, Sn, Zn) on structures, properties and catalytic performance of RuB/γ-Al_2O_3 catalyst was studied using in situ XRD, TEM, H_2-TPD, XPS and liquid-phase hydrogenation of ethyl lactate to 1,2-propanediol (PDO). It was found that incorporation of Sn or Fe improved the dispersion and thermal stability of RuB. The electron density of Ru and the strength and capacity of H_2 adsorption on the RuB catalyst were also enhanced by the incorporation of Sn or Fe. The incorporation of Co or Zn led to a significant decrease in H_2 adsorption capacity of the RuB catalyst. Both ethyl lactate conversion and selectivity to 1,2-PDO increased with the incorporation of Sn or Fe. The ethyl lactate conversion decreased sharply with the incorporation of Zn or Co accompanied by an increase in selectivity to 1,2-PDO and lactic acid. The effect of promoters on reaction behavior was discussed on the basis of the characterizations.

Keywords: RuB/γ-Al_2O_3 catalyst; Promoting effect; Structures; Ethyl lactate hydrogenation

1. Introduction

1,2-Propanediol (PDO), a material that has been widely used in pharmaceutical and chemical industries is commercially produced by the hydration of propylene oxide that is produced via the oxidation of propylene. This process involves either hydroperoxidation chemistry or the antiquated chlorhydrin process [1]. Development of alternative green processes for the synthesis of 1,2-PDO has attracted great attentions. It is reported that 1,2-PDO is formed by the transesterification of propylene carbonate with methanol using solid base catalysts, in which equimolar amount of dimethyl carbonate is co-generated [2]. The co-generation of two compounds makes the transesterification process very complicated and economically uncompetitive. Zhang et al. [3] and Cortright et al. [4] reported that 1,2-PDO can be synthesized via direct hydrogenation of lactic acid using Ru/C and Cu/SiO_2 catalysts; lactic acid can be produced through the fermentation of a number of renewable resources such as carbohydrates derived from agricultural crops and biomass streams [5,6]. This process provides a clean and economic approach to the synthesis of 1,2-PDO from renewable carbohydrate feedstock instead of from non-renewable petroleum.

Hydrogenation of free carboxylic acids to the corresponding alcohols is more difficult than the hydrogenation of corresponding esters and aldehydes, not only because reactivity of the carbonyl group of the acids is lower than that of the corresponding esters and aldehydes but also acids are reactive with the alcohol product, leading to the formation of esters. Therefore, it is advisable to convert acids to esters before hydrogenation. Hydrogenations of carboxylic acids and esters to the corresponding alcohols are often carried out under vigorous reaction conditions due to weak polarisability and intrinsic steric hindrance of the C=O bond [7]. However, for lactic acid and lactates that contain a reactive hydroxyl group, high reaction temperature is undesirable because it may

* Corresponding authors. Tel.: +86 21 65643977; fax: +86 21 65641740.
E-mail addresses: sryan@fudan.edu.cn (S. Yan), knfan@fudan.edu.cn (K. Fan).

1381-1169/$ – see front matter © 2004 Elsevier B.V. All rights reserved.
doi:10.1016/j.molcata.2004.12.016

lead to side reactions such as polymerization, dehydration, transesterification, and consequently to a decrease in selectivity to 1,2-PDO [3,4]. Therefore, development of active catalysts capable of hydrogenating lactic acid or lactates to 1,2-PDO under mild conditions is of great importance.

Ru-based catalysts, due to its good intrinsic hydrogenation activity for carbonyl compounds, have received great attention in the hydrogenation of a wide range of carboxylic acids and esters. Ru-based catalysts with different supports or different preparation methods have been studied extensively by a number of researchers [8–18]. Promoting effect of tin on the ruthenium has also been studied intensively by several research groups [17–24]. It is found that addition of tin significantly enhanced the selectivity to the corresponding alcohol. Addition of platinum to Ru–Sn catalyst can further improve the catalytic performance in the hydrogenation of carboxylic acids [25]. A widely accepted explanation for the promoting effect of tin is that the active species of tin in ionic form plays a role of activating the carbonyl group by adsorption of carbonyl oxygen, facilitating the attack of carbonyl carbon by the hydrogen atom on adjacent ruthenium site. To our knowledge, effect of promoters other than tin on Ru-based catalysts for hydrogenation of carboxylic acids has not been reported.

In the present work, RuB/γ-Al_2O_3 has been prepared by a novel chemical reduction method. Effect of promoters (Fe, Sn, Co and Zn) on composition, structure and properties as well as catalytic performance in the hydrogenation of ethyl lactate of RuB/γ-Al_2O_3 catalyst has been investigated.

2. Experimental

2.1. Catalyst preparation

The monometallic ruthenium catalyst RuB/γ-Al_2O_3 (labeled as RuB) was prepared by a novel reductant impregnation method described below. A weighed amount of γ-Al_2O_3 was immersed into a 3.0 M potassium borohydride solution at 298 K for 15 min. The excessive solution was decanted and an aqueous solution of $RuCl_3$ was poured into a flask containing the impregnated γ-Al_2O_3 to start the reduction. The molar ratio of KBH_4 to Ru is 6:1. The mixture was kept undisturbed at 298 K until bubble generation ceased. The resulting black solids were washed with distilled water to neutrality and then with absolute alcohol three times to replace water. The solids were then kept in absolute alcohol for characterizations and activity test.

The bimetallic catalysts RuMB/γ-Al_2O_3 (labeled as RuMB, M = Zn, Co, Fe or Sn) were prepared in a similar procedure to that for the RuB catalyst except that the mixed solutions containing desired concentrations of $RuCl_3$ and the corresponding metal chlorides of the promoter were used. The molar ratio of KBH_4 to (Ru + M) is 6:1. The precursors for promoters Zn, Co, Fe and Sn were $ZnCl_2$, $CoCl_2{\cdot}6H_2O$, $FeCl_3{\cdot}6H_2O$, and $SnCl_2{\cdot}2H_2O$ of analytical purity, respectively.

2.2. Characterizations

The bulk compositions of the catalysts were analyzed by inductively coupled plasma (ICP, IRIS Intrepid).

The Brunauer–Emmett–Teller surface areas (S_{BET}) of the as-prepared catalysts were determined by N_2 adsorption at 77 K in a Micromeritics TriStar 3000 apparatus. Samples with the storage liquid were transferred to the adsorption glass tube and treated at 383 K under ultrahigh purity nitrogen flow for 2 h before measurement. The samples were weighed by the difference in the adsorption tube on completion of the experiment.

The in situ powder X-ray diffraction (XRD) patterns were acquired on a Bruker AXS D8 Advance X-ray diffractometer using Ni-filtered Cu Kα radiation (λ = 0.15418 nm). The tube voltage and current were 40 kV and 40 mA, respectively. The sample with solvent was loaded in the in situ cell, with argon flow (99.9995%) purging the sample throughout the detection to avoid oxidation.

The temperature-programmed desorption of hydrogen (H_2-TPD) experiment was performed in a flow system using a thermal conductivity detector (TCD) to monitor H_2 desorption. Prior to H_2 adsorption, the sample was treated at 423 K for 2 h under argon flow (99.9995%, deoxygenated by an Alltech Oxy-trap filter), then cooled down to room temperature. The saturation chemisorption of hydrogen was performed by pulse injection until the eluded peak area leveled off. The sample was purged with argon again and was heated at a rate of 20 K min^{-1}, when a steady level of baseline was achieved. An additional H_2-TPD experiment for RuSnB/γ-Al_2O_3 was also performed, in which the conditions for catalyst pretreatment and TPD were the same as those mentioned above except that a Stanford Research Systems QMS Series Gas Analyzer instead of a TCD was used to monitor hydrogen. The TPD profile obtained using the gas analyzer including the shape and peak temperature was almost the same as that observed by TCD.

The X-ray photoelectron spectroscopy (XPS) experiment was carried out on a Perkin-Elmer PHI 5000C ESCA using Al Kα line as the excitation source ($h\nu$ = 1486.6 eV). The sample was pressed into a self-supported disc before being mounted on the sample plate. Then it was degassed in the pretreatment chamber at 383 K for 2 h in vacuum before being transferred into the analyzing chamber, where the background pressure was lower than 2×10^{-9} Torr. All the binding energy (BE) values were obtained after removing the surface oxides by Ar^+ sputtering and were referenced to the Al 2p line of the γ-Al_2O_3 support at 74.4 eV with an uncertainty of ±0.2 eV. The XPS peaks were decomposed into subcomponents using a Gaussian–Lorentzian curve-fitting program.

Transmission electron microscopy (TEM) images were recorded on a JEOL JEM 2011 electron microscope operating at 200 kV. The catalyst specimens for electron microscopic analysis were prepared by gently grinding the powder samples in an agate mortar, suspending and sonicating the powder in alcohol, and placing a drop of the suspension on

a holey carbon copper grid. The amorphous character of the as-prepared catalysts was verified by selected-area electron diffraction (SAED).

2.3. Activity test

The catalytic reaction was carried out in a 220 mL stainless steel autoclave equipped with a magnetic stirrer. In a typical experiment, 5 mL of ethyl lactate, 30 mL of *n*-heptane as solvent and 2.0 g of catalyst were charged into the reactor. The reactor was purged with hydrogen four times to expel air. After the desired temperature, 423 K, was reached, H_2 was pressurized to 5.5 MPa and the stirring (1000 rpm) was commenced. The reaction was allowed to proceed for 10 h with sampling of a small portion of the reaction mixture every 1 h. The reaction products were analyzed with a gas chromatograph equipped with a capillary column PEG-20M (50 m × 0.32 mm) and a flame ionization detector.

3. Results and discussion

3.1. Effect of promoters on the composition and structure of the RuB catalyst

Table 1 lists the compositions, surface areas and particle sizes of the RuB catalyst doped with different promoters. It is found from Table 1 that the BET surface area of the catalyst decreases slightly after incorporation of zinc or cobalt and remains unchanged after incorporation of tin or iron. The loading amount of Ru determined by ICP decreases slightly with the incorporation of promoters. Meanwhile, the Ru/B ratio of the catalyst decreases slightly with the incorporation of zinc or cobalt, and it decreases by higher than 50% after incorporation of tin or iron, which indicates that the content of boron in the catalyst is increased significantly after the incorporation of tin or iron. According to the literature [26], the following three independent reactions may take place in the system during reduction of metal chlorides with potassium borohydride:

$$BH_4^- + 2H_2O \rightarrow BO_2^- + 4H_2 \uparrow \quad (1)$$

$$nBH_4^- + 4M^{n+} + 2nH_2O \rightarrow 4M \downarrow + nBO_2^- + 4nH^+ + 2nH_2 \uparrow \quad (2)$$

$$BH_4^- + H_2O \rightarrow B \downarrow + OH^- + 2.5H_2 \uparrow \quad (3)$$

Besides the above reactions, the following reaction could occur under the conditions used:

$$M^{n+} + nOH^- \rightarrow M(OH)_n \downarrow \quad (4)$$

Due to the different reduction potentials of the precursors and the different solubility product of the hydroxide of the promoters, the rates of the above four reactions and hence their contributions to the overall reaction and to the final catalyst are likely to change. Such differences would influence the chemical state of the promoter as well as the Ru/B ratio of the final catalyst, as observed in Table 1.

The TEM images of RuB catalysts with different promoters and a typical SAED pattern of the catalyst are shown in Fig. 1. Both RuB and RuMB catalysts prepared by reductant impregnation are amorphous, as only a diffraction halo is observed in the SAED pattern (Fig. 1f). The non-promoted RuB catalyst exhibits a scattered RuB particle size distribution ranging from 30 to 66 nm with a mean particle size of 56 nm.

Incorporation of promoter leads to a drastic decrement of the RuB particle size and to a narrowing range of the particle size distribution. Due to the high surface energy of the nanosized amorphous alloys, metal–metalloids prepared by chemical reduction with borohydride or hypophosphite are inclined to aggregate to form larger particles with diameters of several 10s to several 100s of nanometers [27]. The present observation demonstrates that the addition of promoters inhibits the aggregation of RuB, leading to a higher dispersion of the RuB particles. Moreover, the mean sizes of the RuB particles in the tin or iron-promoted catalysts are smaller than those in the zinc or cobalt-promoted catalysts, as shown in Fig. 1 and Table 1.

Fig. 2 shows the typical XRD patterns of the as-prepared RuB and RuSnB catalysts. Besides the peaks corresponding to γ-Al_2O_3, a weak and broad peak centered at $2\theta = 44^\circ$, indicative of amorphous Ru, is observed for the as-prepared RuB catalyst. This is in accordance with the SAED patterns of the catalysts. The XRD patterns of the as-prepared catalyst do not change noticeably after addition of promoters. The broad peak, indicative of the amorphous Ru, remains. After treatment at 573 K as shown in Fig. 3, the intensity of the diffraction peak at $2\theta = 44^\circ$ increases while the width of the peak decreases for both the non-promoted RuB and the

Table 1
Compositions and physical properties of the RuB and RuMB catalysts

Catalyst code	Bulk composition (atomic ratio)	Ru loading (wt.%)	Ru/B (atomic ratio)	M/Ru (mol%)	S_{BET} ($m^2\ g^{-1}$)	*d*p (nm)[a]
RuB	$Ru_{68.2}B_{31.8}$	4.7	2.14	–	165	56.0
RuZnB	$Ru_{58.5}Zn_{8.1}B_{33.4}$	4.1	1.75	13.9	163	14.3
RuCoB	$Ru_{60.9}Co_{8.6}B_{30.5}$	4.5	2.00	14.1	160	13.1
RuFeB	$Ru_{45.6}Fe_{6.5}B_{47.9}$	4.0	0.95	14.3	166	9.1
RuSnB	$Ru_{41.0}Sn_{5.1}B_{53.9}$	4.2	0.76	12.4	165	9.4

[a] Measured by TEM.

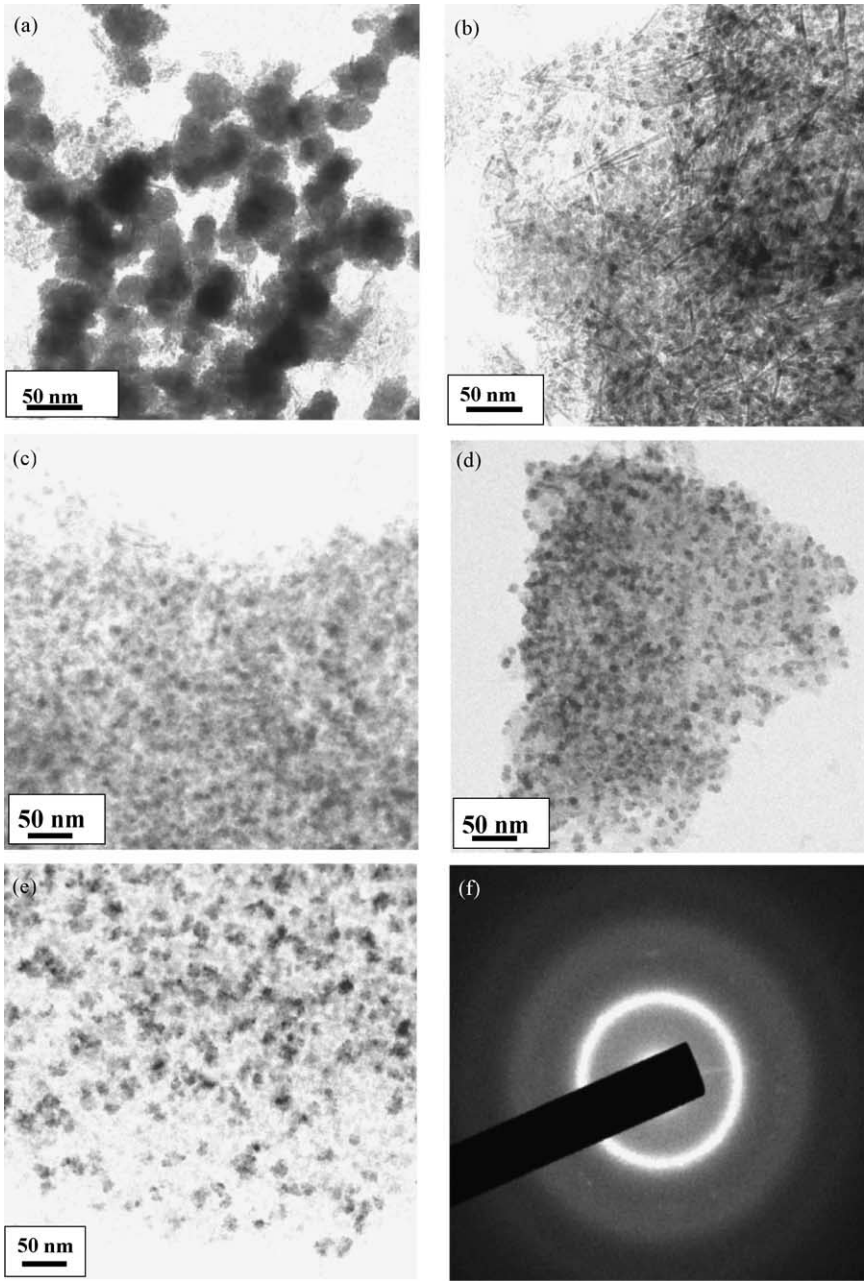

Fig. 1. TEM images of RuB (a); RuZnB (b); RuCoB (c); RuFeB (d); RuSnB (e) and SAED pattern or RuB (f).

cobalt or zinc promoted catalysts. However, the XRD patterns of the iron or tin-promoted catalysts retain the typical amorphous feature even after treatment at 573 K. The in situ XRD experiment indicates that the addition of tin or iron inhibits the crystallization of the amorphous RuB, leading to the improvement in thermal stability of the catalyst, whereas the incorporation of zinc or cobalt could not improve the thermal stability of RuB. This seems to imply that the location and chemical state of tin and iron in the catalyst should be different from those of zinc and cobalt, and hence the interactions between RuB and tin (or iron) should be different from those between RuB and zinc (or cobalt).

3.2. Effect of promoters on the electronic properties of the catalyst

Fig. 4 shows the XPS peaks of Ru 3d and B 1s core levels of the RuB and RuMB catalysts, respectively. The curve-fitting results of the XPS peaks of Fe, Zn, Sn and Co are listed in Table 2. As the peak of Ru $3d_{3/2}$ overlaps with that of C 1s, the peak of Ru $3d_{5/2}$ was employed for all the catalysts to determine the chemical state of Ru. Fig. 4 shows that Ru species in all catalysts are present in the metallic state with binding energy (BE) values falling in the range between 279.1 and 279.6 eV, in accordance with the values of metallic

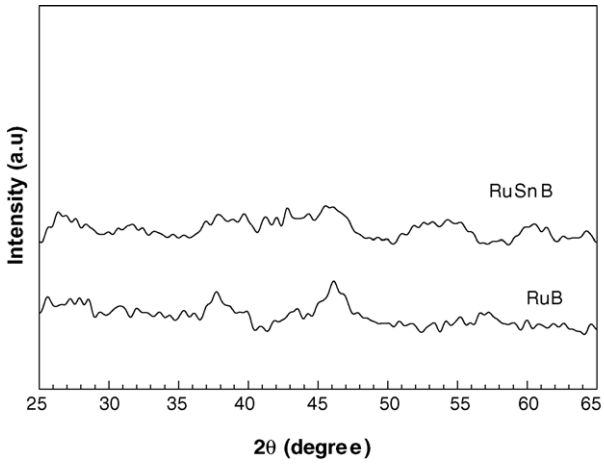

Fig. 2. XRD patterns of the as-prepared RuB and RuSnB catalysts.

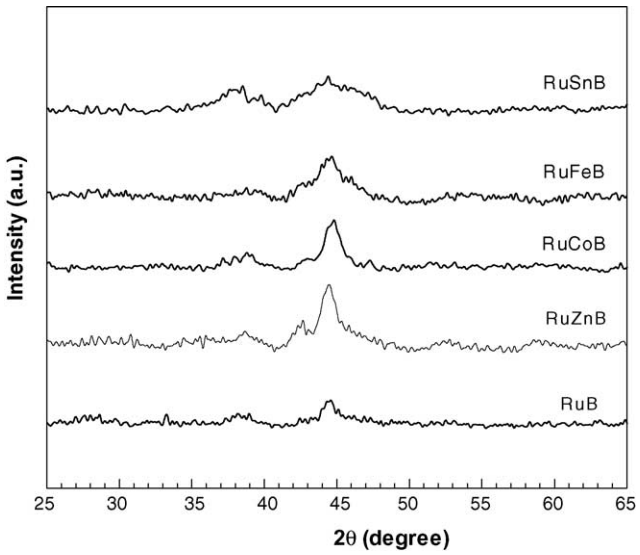

Fig. 3. XRD patterns of the catalysts after treatment at 573 K under argon flow.

Table 2
Curve-fitting results of M for RuMB catalysts

Catalyst	M	BE (eV)	Species	Concentration (%)
RuZnB	Zn LMM	992.3	Zn^{2+}	100
RuCoB	Co 2p3/2	780.8 (785.7)	Co^{2+}	53
		777.5 (773.9)	Co	47
RuFeB	Fe 2p3/2	711.1 (720.8)	Fe^{3+}	38
		708.8 (715.9)	Fe^{2+}	36
		706.0	Fe	26
RuSnB	Sn 3d5/2	486.6	Sn^{2+}	90
		485.2	Sn	10

Ru reported in the literature [21,27,28]. Meanwhile, for both the non-promoted and zinc-promoted RuB catalysts, a peak at BE of 274.4 eV appears in addition to the Ru $3d_{5/2}$ peak at BE of 279.5 eV, which may suggest the existence of two states of the metal with different dispersion and consequently different charging effect on the surface [29]. The difference in binding energy between the two states may be explained by the difference of the charge effect.

Only two Ru peaks are observed for the catalysts incorporated with cobalt, iron or tin. The curve-fitting results of Ru peaks show that compared with the value of the non-promoted RuB catalyst the BE of Ru $3d_{5/2}$ shifts negatively by 0.1–0.2 eV after the addition of zinc or cobalt, and by more than 0.4 eV after the addition of tin or iron. This suggests that the electron density of Ru is increased with addition of the promoter, and this shift is more pronounced when tin or iron is used as a promoter. The XPS spectra of boron species in all catalysts mainly exhibit two oxidation states. The peak at BE of 188.8–189.7 eV is indicative of the elemental boron, while

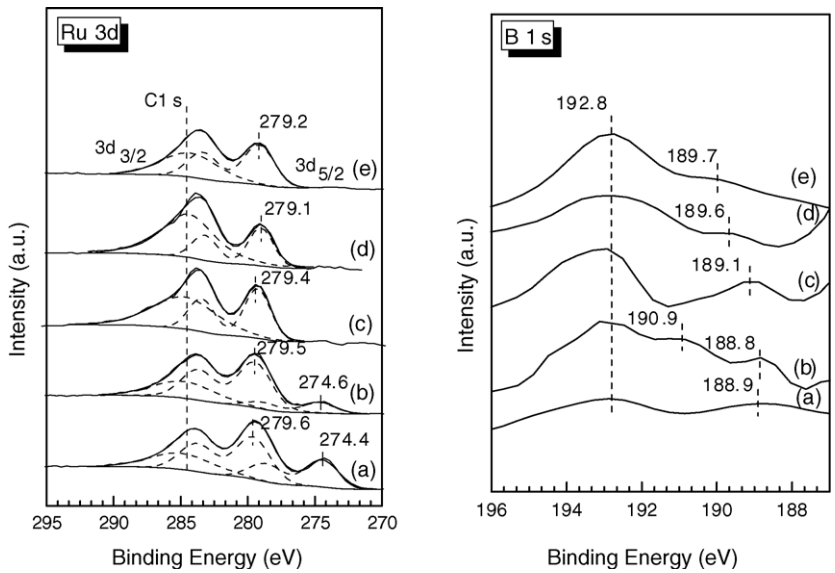

Fig. 4. XPS spectra of Ru 3d and B 1s for RuB (a), RuZnB (b), RuCoB (c), RuFeB (d) and RuSnB (e).

the peak at BE of 192.8 eV is attributed to the oxidized boron in the form of B_2O_3 [27,28]. The BE of elemental boron in the promoted catalysts shifts positively from the value in the non-promoted RuB catalyst. Especially, for the RuFeB and RuSnB catalysts, the BE of element boron shifts positively by more than 0.7 eV. The positive shift of the BE of elemental boron in association with the negative shift of the BE of Ru implies that addition of tin or iron enhances the partial electron transfer from boron to ruthenium, making ruthenium electron-enriched and boron electron-deficient. The negative shift of ruthenium BE for zinc or cobalt-promoted catalysts is much smaller than that for the tin or iron-promoted catalysts.

The more pronounced negative shift of ruthenium BE for the tin or iron-promoted catalysts might be related to their higher B/Ru ratios than those of zinc- or cobalt-promoted catalysts, as shown in Table 1. The electron transfer from boron to the alloyed metal was also observed over CoB and NiB alloys [30,31].

The curve-fitting results of the XPS peaks of tin, zinc, iron and cobalt are shown in Table 2. It is found that all zinc exists in the oxidized state in the RuZnB catalyst. In the RuSnB catalyst, 90% of tin exists in the oxidized state. Although the difference in BE between Sn^{2+} and Sn^{4+} is too small to be distinguished by XPS, we speculate that the oxidized tin species are mainly Sn^{2+} because $SnCl_2$ is used as a precursor and the catalyst is prepared in the presence of reducing agent. In the RuFeB catalyst, more than 70% of iron exists in the oxidized states (Fe^{2+} and Fe^{3+}). In the RuCoB catalyst, roughly half of cobalt exists in the oxidized and half in the elemental state. The different chemical states of the promoter may be caused by the different reduction potentials of their precursors and different solubility product of their hydroxides, as discussed in Section 3.1, and the different chemical states of promoter in turn may influence the properties and catalytic behavior of the catalyst.

3.3. Effect of promoters on the hydrogen adsorption

Fig. 5 shows the H_2-TPD profiles of the catalysts incorporated with different promoters, in which the signal is normalized based on unit mass. Four H_2 desorption peaks at 550, 616, 694 and 740 K are observed for the non-promoted RuB catalyst, indicating four types of the adsorbed hydrogen species with different bonding strength. Only three H_2 desorption peaks are observed for the promoted catalysts, implying that the homogeneity of ruthenium dispersion is improved with the addition of promoters. This is in accordance with the TEM observation. Fig. 5 also shows that compared with the non-promoted RuB catalyst, the hydrogen adsorption capacity is increased by 60 and 54%, respectively, after addition of iron and tin.

In contrast, the integrated peak areas are decreased by 30 and 20%, respectively, with the addition of zinc and cobalt. Further analysis of the desorption peaks shows that the addition of tin and iron increases mainly the proportion of

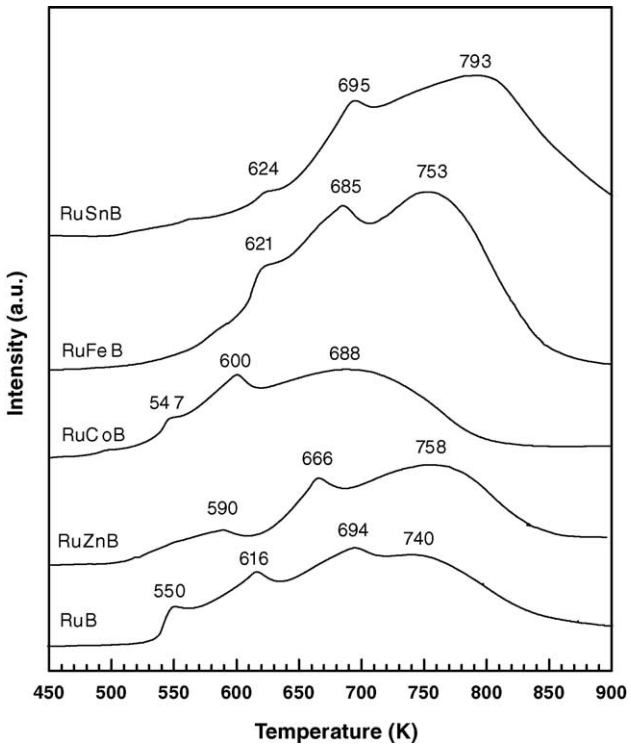

Fig. 5. H_2-TPD profiles of the RuB catalyst with different promoters.

strongly adsorbed species. Moreover, the highest peak temperature shifts from 740 K of the non-promoted RuB to 758, 753 and 793 K, respectively, with the addition of zinc, iron and tin. It shifts to 688 K with the addition of cobalt. The H_2-TPD experiment clearly demonstrates that the capacity of hydrogen adsorption of the catalyst is enhanced by the addition of tin or iron, but is reduced by the addition of zinc or cobalt.

The strength of hydrogen adsorption on the catalyst is enhanced with the addition of zinc, tin or iron, but is reduced with the addition of cobalt. The capacity of hydrogen adsorption is related to the concentration of the exposed metallic sites (Ru) on surface, while the bonding strength of hydrogen is related to the electron density of the ruthenium.

The H_2-TPD experiment seems to imply that tin and iron may be predominantly located between two adjacent RuB clusters, in which the role of tin or iron is a spacer that separates the RuB particles from their neighbors and inhibits their aggregation, in accordance with the in situ XRD results which show that the thermal stability of the RuB catalyst is improved with the addition of tin or iron. On the other hand, the decreased peak area of hydrogen desorption with the addition of cobalt or zinc appears to imply that a great proportion of zinc and cobalt may be over the RuB clusters, leading to partial blockage of ruthenium sites. This is in agreement with the in situ XRD results as the addition of cobalt or zinc produces little improvement in thermal stability of the RuB catalyst.

Table 3
Effect of promoters on the catalytic performance of RuB for the hydrogenation of ethyl lactate[a]

Catalyst code	Conversion (%)	Selectivity (%)			
		1,2-PDO	Lactic acid	2-Hydroxyl propyl lactate	*n*-Propanol + i-propanol
RuB	78.7	50.7	0.5	0.4	48.4
RuZnB	28.5	82.9	9.6	2.1	5.4
RuCoB	51.0	60.3	4.9	0.6	34.2
RuFeB	87.3	80.1	0.1	0.1	19.6
RuSnB	86.2	85.1	10.5	1.4	3.0

[a] Reaction conditions: catalyst 2 g; ethyl lactate 5 mL; *n*-heptane 30 mL; temperature 423 K; hydrogen pressure 5.5 MPa; time 10 h.

3.4. Effect of promoters on the catalytic performance RuB in hydrogenation of ethyl lactate

Table 3 lists the results of liquid phase ethyl lactate hydrogenation using RuB and RuMB catalysts under identical reaction conditions. An ethyl lactate conversion of 78.7% is achieved at 1,2-PDO selectivity of 50.7% by using the non-promoted RuB catalyst. The ethyl lactate conversion increases with the addition of iron or tin, while it decreases sharply with the addition of zinc or cobalt. As far as the reaction selectivity is concerned, it is found that selectivity to 1,2-PDO increases while the selectivity to propanol decreases after addition of the promoter studied in this work. This change is especially pronounced when zinc, tin or iron is used as a promoter. Meanwhile, the selectivity to lactic acid and 2-hydroxylpropyl lactate is increased significantly with the incorporation of zinc or tin. Another interesting point in Table 3 is that although the conversion of ethyl lactate greatly differs between zinc- and tin-promoted catalysts, the selectivity of the products is quite similar. Based on the products formed, a possible reaction pathway is proposed in Scheme 1.

According to the literature [18], acids are some of the primary products from the hydrogenation of esters, and the hydrogenation of acids also gives alcohols. But the reactivity of acids is lower than that of corresponding esters [17]. Therefore, if 1,2-PDO was formed by a consecutive process, i.e. the hydrolysis of ethyl lactate followed by hydrogenation of lactic acid, there would be a considerable concentration of lactic acid in the product spectrum over a wide range of conversion level. However, it was shown that selectivity to lactic acid over non-promoted RuB and iron- or cobalt-promoted catalysts was very low. Thus, we consider that 1,2-PDO was formed mainly via a direct hydrogenation of ethyl lactate.

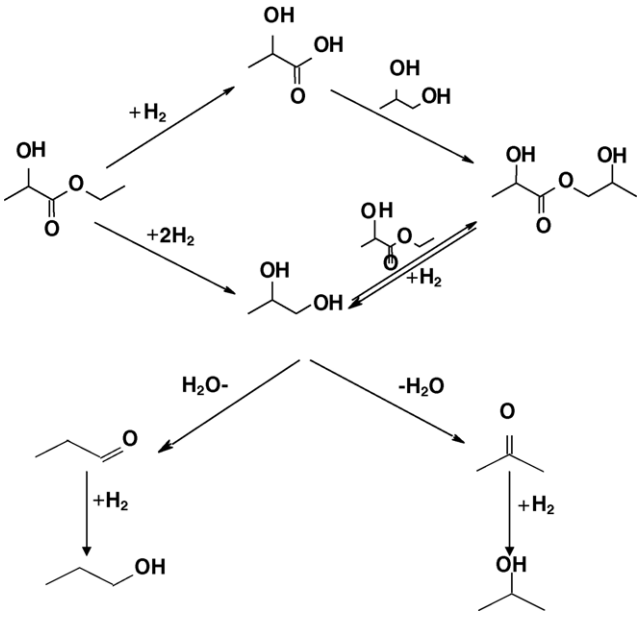

Scheme 1. Possible reaction pathway in the hydrogenation of ethyl lactate.

By comparing the catalytic performance shown in Table 3 with the characterization results, it is found that ethyl lactate conversion is related to the H_2 adsorption capacity of the catalyst. It is explained as follows. It is widely recognized that the hydrogenation of esters proceeds via a Langmuir–Hinshelwood mechanism. Under certain conditions, the conversion of the hydrogenation reaction is dependent upon both concentration of the chemisorbed reactant species on the surface and the chemisorbed hydrogen species available in the vicinity of chemisorbed reactant species. The existence of positively charged species on the surface favors the adsorption and activation of the carbonyl group [21,23], while the formation of highly dispersed electron-rich metallic species is beneficial for the hydrogen activation. For different promoters studied in this work, the proportion of the oxidized species in the promoter inventory and their influence on the dispersion of ruthenium and on hydrogen adsorption are different, which consequently lead to the different reaction performance. When using tin or iron as a promoter, the promoter is present mainly in the oxidized states as shown in Table 2, facilitating the adsorption of carbonyl group of ethyl lactate. Meanwhile, addition of tin or iron enhances the hydrogen adsorption capacity greatly. The combined effect leads to an increase in the ethyl lactate conversion. For cobalt and zinc promoted catalyst, although the oxidized species can enhance the adsorption of carbonyl group, the sharply decreased hydrogen adsorption, as shown in Fig. 5, makes the number of hydrogen species available in the vicinity of the chemisorbed carbonyl group decreased, and hence the conversion of ethyl lactate decrease correspondingly.

The effect of promoters on the selectivity is more complicated. The effect of tin on the ruthenium-based catalyst for hydrogenation of fatty unsaturated esters (or acids) has been discussed by several research groups [17,21,23]. A widely accepted model proposed to explain the effect of tin on the

hydrogenation of C=O is the formation of the oxidized tin species in the atomic closeness to the metallic ruthenium. The role of tin is the activation of the carbonyl group by adsorption of carbonyl oxygen, facilitating the attack of carbonyl carbon by the hydrogen atom on adjacent ruthenium sites [21,23]. The improved selectivity to 1,2-PDO for tin-promoted catalyst may be explained by this model. As for the other three promoters, iron, zinc and cobalt, the correlation of the characterizations with the reaction results shows that selectivity of products is related to the proportion of the oxidized species in the total promoter inventory irrespective of its type. The selectivities to 1,2-PDO, lactic acid and 2-hydroxyl propyl lactate increase while the selectivity to propanols decreases with increasing proportion of the oxidized species in the promoter inventory. The increased selectivity to 1,2-PDO may be explained by the mechanism proposed by Pouilloux et al. [21] and Desphande et al. [23] for the hydrogenation of fatty acid esters using Ru–Sn catalysts. When tin or zinc is used as a promoter, the promoter is mainly in the oxidized state, and part of the promoter species in close contact with ruthenium may act as the adsorption sites for the oxygen atom of the carbonyl in ethyl lactate, leading to the polarization of C=O bond. The metallic ruthenium existing as an electron-rich species activates hydrogen. The activated hydrogen on ruthenium site then attacks the positively charged carbon atom of the carbonyl group. The combined action of ruthenium and the oxidized promoter would result in a significant increase in the selectivity to 1,2-PDO. When cobalt was used as a promoter, 53% of total cobalt is in the oxidized state that could promote the formation of alcohol. Because the proportion of the oxidized species is not as high as that of other three promoters, this promoting effect is less pronounced.

On the other hand, the primary hydrogenation product 1,2-PDO may be adsorbed on the oxidized species if the concentration of the oxidized species is high, and the adsorbed alcoholate, if geometrically permitted, may react with an ester molecules adsorbed on the adjacent sites, leading to the formation of the heavy ester, as observed in Table 3. The higher concentration of the oxidized species favorable for the formation of transesterification product was previously reported by Pouilloux et al. [21] for a Ru–Sn catalyst. The practical reaction mechanism and the pathway of the product formation may be more complicated and are not fully understood.

4. Conclusions

Addition of tin or iron to the RuB catalysts leads to an improvement on RuB dispersion and thermal stability of the amorphous structure. The electron density of ruthenium, the strength and capacity of hydrogen adsorption on RuB are also enhanced by the addition of tin or iron. Addition of zinc or cobalt produces little improvement in thermal stability of the RuB but reduces its hydrogen adsorption capacity. The XPS shows that tin, iron and zinc are mainly present in the oxidized states in the catalyst while nearly 50% of cobalt is present in the elemental state. The catalytic evaluation shows that the addition of tin or iron results in an increase in both ethyl lactate conversion and selectivity to 1,2-PDO while the addition of cobalt or zinc leads to a significant decrease in ethyl lactate conversion accompanied by the increase in selectivity to 1,2-PDO and lactic acid. Correlation of the reaction results with the characterizations shows that the oxidation state of the promoter is very important for the selectivity to 1,2-PDO.

Acknowledgements

This work is supported by the National Basic Research Program of China (2003CB615807, G2000048009), the NSF of China (20203004) and Shanghai Science and Technology Committee (03QB14004).

References

[1] H.H. Szmant, Organic Building Blocks of the Chemical Industry, Academic Press, New York, 1989.
[2] T. Wei, M.H. Wang, W. Wei, Y.H. Sun, B. Zhong, Petrochem. Technol. 31 (2002) 959 (in Chinese).
[3] Z.G. Zhang, J.E. Jackson, D.J. Miller, Appl. Catal. A 219 (2001) 89.
[4] R.D. Cortright, M. Sanchez-Castillo, J.A. Dumesic, Appl. Catal. B 39 (2002) 353.
[5] J.H. Litchfield, Adv. Appl. Microbiol. 42 (1996) 45.
[6] E.S. Lipinsky, R.G. Sinclair, Chem. Eng. Prog. 82 (1986) 26.
[7] A.J. McAlee, J. Chem. Soc. C (1969) 2454.
[8] K. Tahara, H. Tsuji, H. Kimura, T. Okazaki, Y. Itoi, S. Nishiyama, S. Tsuruya, M. Masai, Catal. Today 28 (1996) 267.
[9] M.J. Mendes, O.A.A. Santos, E. Jordão, A.M. Silva, Appl. Catal. A 217 (2001) 253.
[10] K.Y. Cheah, T.S. Tang, F. Mizukami, S. Niwa, M. Toba, Y.M. Choo, J. Am. Oil Chem. Soc. 69 (1992) 410.
[11] K. Nomura, H. Ogura, Y. Imanishi, J. Mol. Catal. A 178 (2002) 105.
[12] K. Ishii, F. Mizukami, S. Niwa, M. Toba, H. Ushijima, T. Sato, J. Am. Oil Chem. Soc. 73 (1996) 465.
[13] K. Tahara, E. Nagahara, Y. Itoi, S. Nishiyama, S. Tsuruya, M. Masai, Appl. Catal. A 154 (1997) 75.
[14] T.S. Tang, K.Y. Cheah, F. Mizukami, S. Niwa, M. Toba, J. Am. Oil Chem. Soc. 71 (1994) 510.
[15] J. Carnahan, T. Ford, W. Gresham, W. Grisby, G. Hager, J. Am. Chem. Soc. 77 (1955) 3766.
[16] S. Antons, B. Beitzke, US Patent 5,536,879 (1996) to Bayer.
[17] M. Toba, S. Tanaka, S. Niwa, F. Mizukami, Z. Koppány, L. Guczi, K.Y. Cheah, T.S. Tang, Appl. Catal. A 189 (1999) 243.
[18] Y. Pouilloux, A. Piccirilli, J. Barrault, J. Mol. Catal. A 108 (1996) 161.
[19] S. Galvagno, A. Donato, G. Neri, R. Pietropaolo, G. Capannelli, J. Mol. Catal. 78 (1993) 227.
[20] M. Agnelli, P. Louessare, A.E. Mansour, J.P. Candy, J.P. Bournonville, J.M. Basset, Catal. Today 6 (1989) 73.
[21] Y. Pouilloux, F. Autin, C. Guimon, J. Barrault, J. Catal. 176 (1998) 215.
[22] V.M. Desphande, W.R. Patterson, C.S. Narasimhan, J. Catal. 121 (1990) 165.
[23] V.M. Desphande, K. Ramnarayan, C.S. Narasimhan, J. Catal. 121 (1990) 174.
[24] G. Luo, S.R. Yan, M.H. Qiao, J.H. Zhuang, K.N. Fan, Appl. Catal. A 275 (2004) 95.

[25] Y. Hara, K. Endou, Appl. Catal. A 239 (2003) 181.
[26] Y. Chen, Catal. Today 44 (1998) 3.
[27] S.H. Xie, M.H. Qiao, H.X. Li, W.J. Wang, J.F. Deng, Appl. Catal. A 176 (1999) 129.
[28] Handbook of X-ray Photoelectron Spectroscopy, Perkin-Elmer Corporation, 1992.
[29] L. Guczi, R. Sundararajan, Zs. Koppány, Z. Zsoldos, Z. Schay, F. Mizukami, S. Niwa, J. Catal. 167 (1997) 482.
[30] Y.G. He, M.H. Qiao, H.R. Hu, J.F. Deng, K.N. Fan, Appl. Catal. A 228 (2002) 29.
[31] X.F. Chen, H.X. Li, H.S. Luo, M.H. Qiao, Appl. Catal. A. 233 (2002) 13.